Mucus physically restricts influenza A viral particle access to the epithelium

Logan Kaler[1,2], Elizabeth M. Engle[2,3], Ethan Iverson[3,4], Allison Boboltz[2], Maxinne A. Ignacio[4], Maria Rife[3,4], Margaret A. Scull[3,4], Gregg A. Duncan[1,2,3*]

[1]Biophysics Program, [2]Fischell Department of Bioengineering, [3]Molecular and Cellular Biology Program, [4]Department of Cell Biology & Molecular Genetics, Maryland Pathogen Research Institute, University of Maryland, College Park, MD 20742

*Correspondence to: Gregg Duncan; email: gaduncan@umd.edu

SUMMARY

Prior work suggests influenza A virus (IAV) crosses the airway mucus barrier in a sialic acid-dependent manner through the actions of the viral envelope proteins, hemagglutinin and neuraminidase. However, host and viral factors that influence how efficiently mucus traps IAV remain poorly defined. In this work, we assessed how the physicochemical properties of mucus influence its ability to effectively capture IAV with altered sialic acid preference using fluorescence video microscopy and multiple particle tracking. We found an airway mucus gel layer must be produced with pores on the order of size of the virus to physically constrain IAV. Sialic acid binding by IAV also improves mucus trapping efficiency, but interestingly, sialic acid preferences had little impact on the fraction of IAV particles expected to penetrate the mucus barrier. Together, this work provides new insights on mucus barrier function toward IAV with important implications on innate host defense and interspecies transmission.

KEYWORDS

Influenza A virus, mucus, sialic acid, diffusion, particle tracking

INTRODUCTION

Airway mucus is the first line of defense against inhaled particulates and pathogens.[1,2] The mucus layer is comprised of mucins, which are heavily glycosylated gel-forming proteins.[3] Mucin glycoproteins possess a bottle-brush architecture where predominantly *O*-linked glycans extend from the peptide backbone and terminate with functional groups such as fucose, sialic acid, and sulfate.[4,5] Mucin-associated glycans make up approximately 70–80% of the total mass of mucin and thus, play a critical in the physical properties of mucus and its biological role in innate lung defense.[4–6] Disulfide bonds between the cysteine-rich domains of the mucins and electrostatic interactions between mucin glycoproteins are responsible for the formation of the mucus gel network.[3] The airway mucus gel effectively traps nano-scale particles and removes them via a process called mucociliary clearance, where cilia on the surface of the cell beat in coordination to move the mucus layer through the airway[3]. Prior work has demonstrated the functional benefits of the mucus barrier in preventing IAV infection. For example, infection by IAV was significantly inhibited in mice with lung-specific overexpression of mucin 5ac (Muc5ac) demonstrating its protective function.[7] By mimicking the seasonal changes in humidity, prior work has also shown decreased air humidity dehydrates airway mucus leading to impaired mucociliary clearance and increased susceptibility to IAV infection in mice.[8] Taken together, the mucus gel acts to directly

block IAV and other viruses from entering the underlying epithelium by facilitating their clearance from the airway.

Prior studies on the mechanisms by which IAV overcomes the mucus barrier has primarily focused on the protective role of mucin-associated sialic acid (Sia).[9] IAV is an enveloped virus with two glycoproteins on the envelope that recognize Sia: hemagglutinin (HA) and neuraminidase (NA).[2,9] HA and NA work cooperatively to initiate infection in the airway epithelium, with HA binding Sia while NA is responsible for solubilizing Sia, favoring HA-Sia dissolution.[9] Sia is found on the surface of the epithelial cells in the respiratory tract as well as on mucins. In prior work, it was found that inhibition of NA leads to immobilization of IAV particles in airway mucus.[10,11] In addition, chemical and/or enzymatic removal of mucin-associated Sia has been shown to enhance the mobility of IAV through mucus.[10,11] This suggests mucin sialylation enables mucus gel trapping of IAV through direct binding by HA and release of Sia by NA enables IAV to efficiently bypass the mucus barrier. However, this past work did not consider the physical constraints imposed by mucus as a hydrogel with pores ranging in sizes from 100-500 nm on IAV particles, with a diameter ranging from ~120 nm in a spherical form to ≥250 nm in a filamentous form.[3,12–14] In previous work from our group, we observed IAV diffused in human mucus at a similar rate to synthetic, muco-inert nanoparticles with a diameter comparable to IAV.[15] This would suggest the mucus barrier acts to physically block the penetration of IAV rather than adhesively trap mucus through IAV binding to Sia. It should be noted another study also observed little evidence of Sia-mediated trapping of IAV within mucus and alternatively proposed that neutralizing antibodies against IAV facilitate entrapment in the mucus barrier.[16] Considering these past observations by ourselves and others, the features of mucus that render it permissive to IAV particles has yet to be clearly established. Further, the role of binding preference for α2,3- or α2,6-Sia on IAV trapping within mucus is largely unaddressed. We also note prior reports have shown airway mucins in a soluble form can competitively inhibit infection by IAV and other viruses.[17,18] We consider these direct antiviral effects as distinct from mucus gel barrier functions that facilitate capture and removal of viral particles from the airway.

In this work, we used A/Udorn/307/72 (Udorn), a H3N2 IAV that possesses pleomorphic particle morphologies with both spherical and filamentous shape, to study how IAV navigates through airway mucus with physically and biochemically distinct barrier properties. To study the impact of sialic acid preference on IAV penetration through mucus, we evaluated the diffusion of Udorn IAV with mutations to specific residues in the receptor binding domain that alter its preference to either α2,3- or α2,6-Sia.[19,20] Our previous study was conducted using *ex vivo* human airway mucus collected from patients to evaluate IAV diffusion through mucus.[15] However, the properties of mucus samples vary significantly from patient-to-patient. To provide a source of mucus with more consistent properties, we harvested mucus from different human airway epithelial cell (HAE) lines, in addition to normal human bronchial epithelial (NHBE) primary cells for this work. Mucus collections from 3 different lung epithelial cell sources allowed us to compare their ability to trap IAV and how this may relate to their biomolecular properties.

RESULTS

Biochemical characterization of human lung epithelial cell-derived mucus

To study the mobility of IAV within human airway mucus, lung epithelial cells grown at an air-liquid interface (ALI) were used to generate mucus which could be regularly collected for

experimental use. Mucus collected from Calu-3, BCi-NS1.1 (BCi),[21] and NHBE cultures was characterized for relative mucin content, Sia concentration, and disulfide bond (cystine) concentration using fluorometric assays **(Figure 1A-C)**. NHBE mucus possessed significantly higher concentrations of mucin, Sia, and disulfide bonds in comparison to both BCi and Calu-3 mucus. In comparison to Calu-3 mucus, relative mucin content was ~1.8-fold higher in BCi mucus **(Figure 1A)**. There were no significant differences in the disulfide bond and Sia concentration between BCi and Calu-3 mucus **(Figure 1C)**.

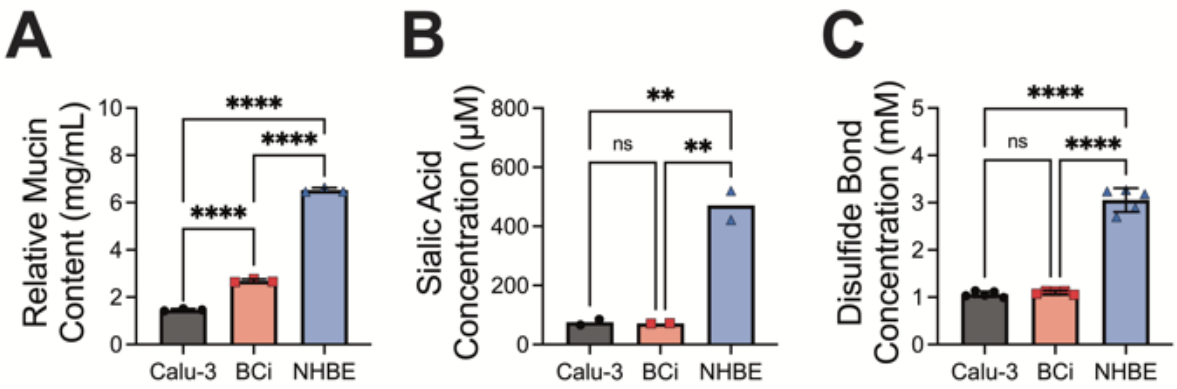

Figure 1. Biochemical characterization of human lung epithelial cell-derived mucus. (A-C) Characterization of Calu-3, BCi, and NHBE mucus to determine **(A)** relative mucin content, **(B)** Sia concentration, and **(C)** disulfide bond concentration. Bars indicate mean with error bars for standard deviation with measurements shown as points. Data set statistically analyzed with one-way ANOVA and Šídák's multiple comparisons test: ns = not significant; $^{**}p < 0.01$, $^{****}p < 0.0001$.

Udorn IAV and size-matched nanoparticle diffusion in airway mucus

The diffusion of muco-inert nanoparticles (NP) and fluorescently-labeled Udorn IAV was assessed in mucus harvested from Calu-3, BCi, and NHBE ALI cultures **(Figure 2A)**. We confirmed muco-inert NP and Udorn IAV possessed comparable particle size based on dynamic light scattering measurements (**Figure S1**). Thus, muco-inert NP serve as an experimental control that indicate the potential impact of mucus microstructure on IAV trapping. Diffusion rates measured for both NP and Udorn IAV were determined in the same regions of interest using fluorescence video microscopy. Multiple particle tracking analysis of NP indicated the resulting diffusion rate of NP, as measured by the $\log_{10}[MSD_{1s}]$, was the highest in Calu-3 mucus and the lowest in BCi mucus **(Figure 2B)**. Based on measured NP diffusion, we estimated the pore size of the mucus network **(Figure 2C)**. For comparison to the estimated mucus pore sizes, the size range of Udorn IAV particles measured by dynamic light scattering is also highlighted in gray. Calu-3 mucus possessed the largest pores ranging from 1000–2000 nm (**Figure 2C**). In comparison, BCi and NHBE mucus pore sizes were much smaller with values ranging from approximately 200–900 nm and 350–950 nm, respectively. Particle tracking analysis showed Udorn particle diffusion was significantly increased in Calu-3 mucus compared to both NHBE and BCi mucus **(Figure 2D)**. In addition, we observed Udorn IAV diffusion in BCi mucus was significantly reduced in comparison to NHBE mucus.

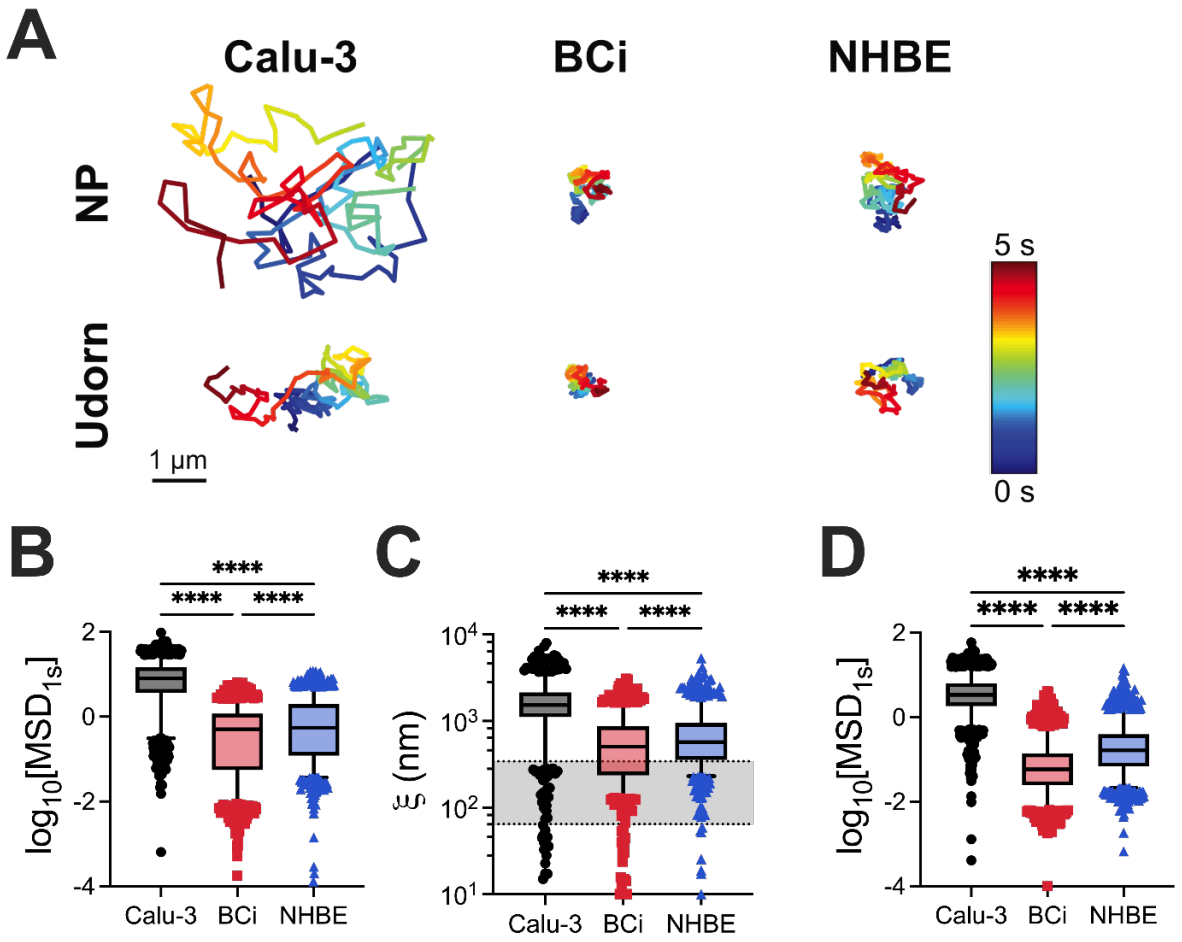

Figure 2. Udorn IAV and size-matched nanoparticle diffusion in airway mucus. (A) Representative trajectories for diffusion of NP and Udorn in Calu-3, BCi, and NHBE mucus. Trajectory color changes with time, with dark blue indicating 0 s and dark red indicating 5 s. Scale bar = 1 μm. **(B)** Measured $\log_{10}[MSD_{1s}]$ for NP in Calu-3, BCi, and NHBE mucus. **(C)** Estimated pore size (ξ) from NP diffusion in Calu-3, BCi-NS1.1, and NHBE mucus. Shaded region indicates size range of Udorn particles as measured by dynamic light scattering. **(D)** Measured $\log_{10}[MSD_{1s}]$ for Udorn in Calu-3, BCi, and NHBE mucus. Whiskers are drawn down to the 5th percentile, up to the 95th percentile, and outliers are plotted as points. Data sets statistically analyzed using Kruskal-Wallis test with Dunn's test for multiple comparisons: ****$p < 0.0001$. Data for Calu-3 is shown as black circles, BCi is shown as red squares, NHBE is shown as blue triangles.

Impact of enzymatic sialic acid depletion on IAV diffusion through mucus

To evaluate the role of Sia in IAV diffusion, we enzymatically depleted Sia in NHBE mucus. NHBE mucus was used for these studies given the markedly higher Sia content found in these samples compared to other mucus sources (**Figure 1B**). Exogenous neuraminidase enzyme (NA_{ex}) from *Arthrobacter ureafaciens* was introduced to hydrolyze terminal Sia.[22] Treatment with NA_{ex} resulted in an 8-fold decrease in Sia concentration compared to untreated mucus, resulting in Sia levels comparable to mucus from BCi and Calu-3 cultures **(Figure 3A)**. Multiple particle tracking was used to analyze NP and Udorn movement in untreated and NA_{ex} treated mucus. Representative trajectories and measured $\log_{10}[MSD_{1s}]$ showed that Udorn particles moved at a faster rate in NA_{ex} treated mucus compared to untreated mucus **(Figure 3B,C)**. We also found NP diffused

significantly faster than Udorn in both untreated and NA_{ex} treated NHBE mucus **(Figure 3C)**. However, there was no significant difference in NP diffusion in NA_{ex} treated mucus compared to untreated mucus.

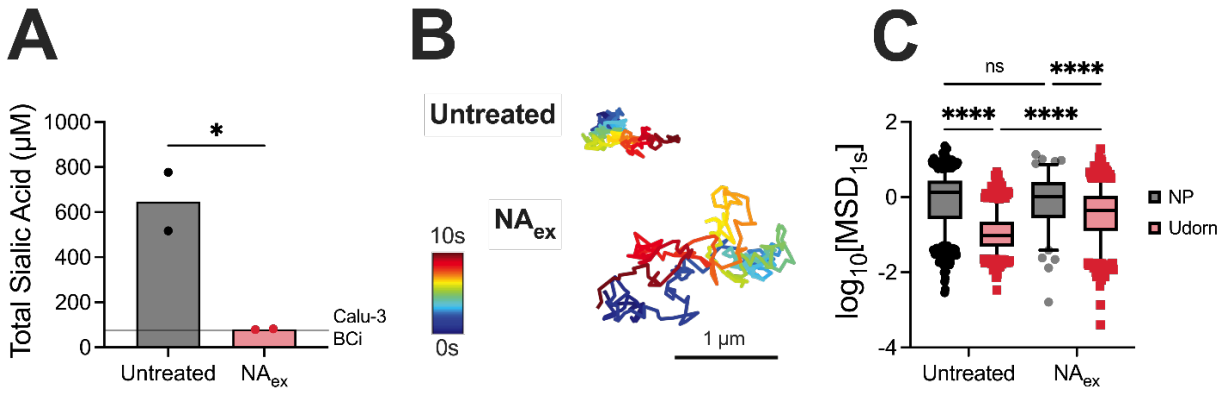

Figure 3. Impact of enzymatic sialic acid depletion on IAV diffusion through mucus. (A) Characterization of total Sia concentration for untreated and NA_{ex} treated NHBE mucus. Lines drawn to indicate levels of Sia measured in Calu-3 and BCi samples from Figure 1. Data set in **(A)** statistically analyzed with an unpaired T-test: *$p < 0.05$. **(B)** Representative trajectories of Udorn in untreated and NA_{ex} treated NHBE mucus. Trajectory color changes with time, with dark blue indicating 0 s and dark red indicating 10 s. Scale bar = 1 μm. **(C)** Measured $\log_{10}[MSD_{1s}]$ for NP and Udorn. Data set in **(C)** statistically analyzed with Kruskal-Wallis test with Dunn's test for multiple comparisons: ns = not significant; ****$p < 0.0001$.

Impact of Sia preference on IAV-mucus interactions and the number of virions predicted to breach the mucus barrier

To probe the impact of Sia binding preference on IAV diffusion, we used two previously established Udorn mutants with preferential binding for either α2,3-Sia (Ud23) or α2,6-Sia (Ud26).[20] Diffusion of each Udorn mutant in NHBE mucus was determined in conjunction with the wildtype Udorn and muco-inert NP. Based on particle tracking analysis, measured $\log_{10}[MSD_{1s}]$ showed a significant increase in Ud26 diffusion compared to Udorn and Ud23 in NHBE mucus **(Figure 4A-B)**. However, NP were significantly more diffusive than all Udorn IAV particle types tested. To gain further insight on the dependence of IAV-mucus interactions on Sia binding preference, a statistical mechanics-based analysis developed in prior work was used to determine an effective dissociation constant (K_{3D}) for Udorn IAV binding to the mucus gel.[15] Interestingly, there were no significant differences in estimated K_{3D} for Udorn, Ud23, and Ud26 in NHBE mucus **(Figure 4C)**. Next, we computationally predicted the time required for each IAV type to penetrate a 10 μm-thick mucus barrier using a machine learning-based approach developed in prior work.[23] First, machine learning was used to classify individual IAV trajectories as either subdiffusive or diffusive. The subdiffusive particles were further classified as exhibiting either fractional Brownian (FBM) or continuous time random walk (CTRW) motion.[24] FBM particles follow a random walk, but the following step has a higher probability to be in the opposite direction than the previous step.[24] CTRW particles are characterized by random jumps in time and space, resulting in a "hopping" motion.[24] Diffusive particles are undergoing Brownian motion (BM), which is classical thermally driven diffusion, characterized as a random walk with steps taken to

the left and right with equal probability.[25] The resulting classification of particles indicated the majority of Udorn, Ud23, and Ud26 particles were exhibiting FBM with a smaller percentage of BM **(Figure 4D-E)**. Interestingly, all IAV strains had some percentage of particles that exhibited CTRW "hopping" movement in NHBE mucus, with Ud26 having the largest percentage of CTRW particles. Based on individual IAV diffusion modes, the percentage of particles to cross the mucus barrier in 60 minutes was mathematically predicted for each Udorn IAV type **(Figure 4F)**. Udorn was predicted to have the largest percentage of particles across the mucus barrier in 60 minutes compared to all other IAV types in NHBE mucus, with ~22%, while Ud23 and Ud26 have predicted percentages of ~16% **(Figure 4F, Supplemental Table 1)**. For all IAV types, particles exhibiting FBM were not predicted to cross the mucus barrier in a physiologically-relevant timeframe.

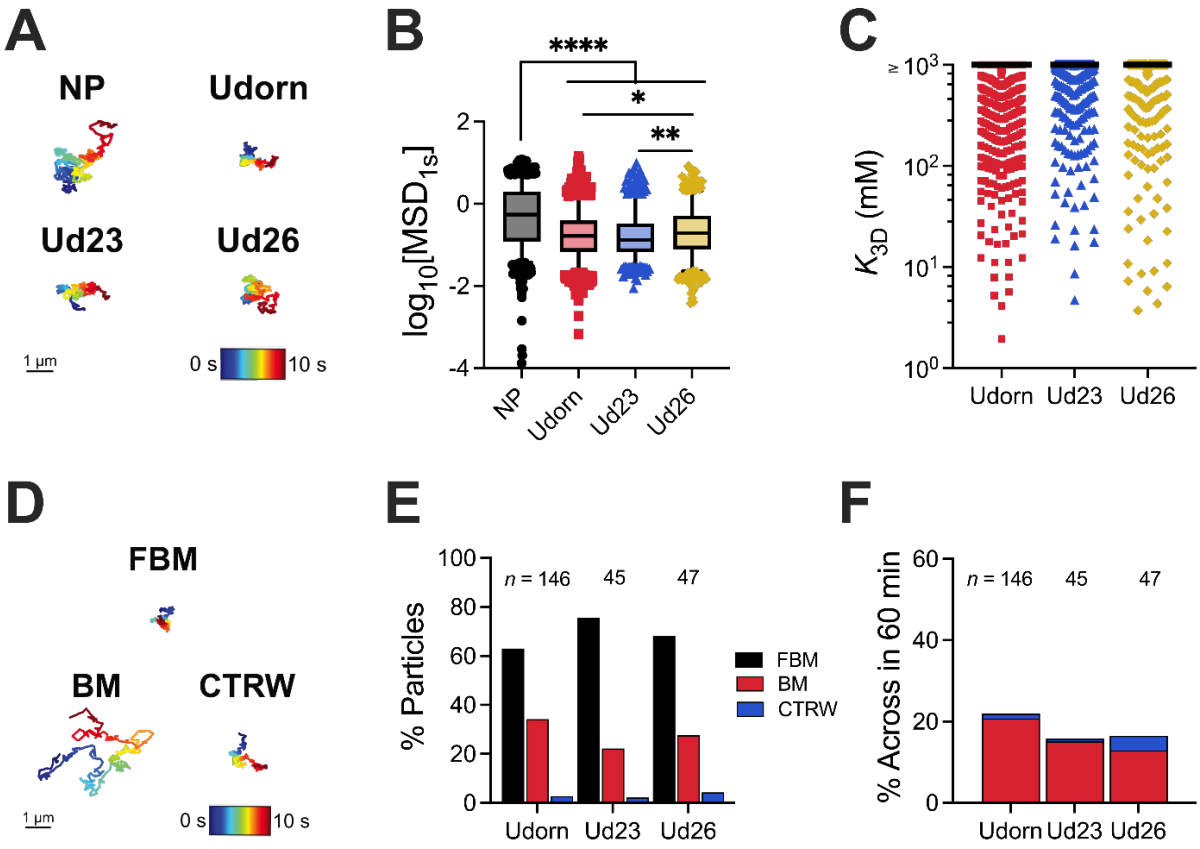

Figure 4. Impact of Sia preference on IAV-mucus interactions and the number of virions predicted to breach the mucus barrier. (A) Representative trajectories for NP, Udorn, Ud23, and Ud26 in NHBE mucus. **(B)** Measured $\log_{10}[MSD_{1s}]$ for NP, Udorn, Ud23, and Ud26. **(C)** Estimated dissociation constants (K_{3D}) for Udorn, Ud23, and Ud26 in NHBE mucus. IAV with a calculated $K_{3D} \geq 1000$ mM are compiled as these high K_{3D} are indicative of negligible IAV-mucus interactions. **(D)** Representative trajectories of Udorn exhibiting FBM, BM, and CTRW diffusion in NHBE mucus. **(E)** Normalized percent of Udorn exhibiting FBM, BM, and CTRW motion in each sample, with the corresponding total number of particles. **(F)** Percent of Udorn particles to cross the 10 μm mucus barrier in 60 minutes for each sample, calculated from the cumulative distribution function and normalized percent of particles. Trajectory color changes with time, with dark blue indicating 0 s and dark red indicating 10 s. Scale bar = 1 μm. Whiskers are drawn down to the 5th percentile, up to the 95th percentile, and outliers are plotted as points. Data set in **(B)** statistically

analyzed with Kruskal-Wallis test with Dunn's test for multiple comparisons: *p < 0.05, **p < 0.01, ****p < 0.0001. In **(B-C)**, NP is shown as black circles, Udorn is shown as red squares, Ud23 is shown as blue triangles, and Ud26 is shown as yellow diamonds. In **(E-F)**, FBM is shown as black bars, BM is shown as red bars, and CTRW is shown as blue bars.

DISCUSSION

In this work, we used video microscopy and multiple particle tracking analysis to evaluate how size-limited transport and adhesive Sia binding influence mucus barrier function towards IAV. We conducted these studies using mucus harvested from 3 commonly used lung epithelial culture models. Our studies revealed significant differences in the biochemical and biophysical properties of mucus produced in each culture. Based on our measurements of NP diffusion **(Figure 2)**, Calu-3 mucus possesses pore sizes on the order of microns which is far larger than what has been previously reported for human airway mucus collected *ex vivo*.[14,26,27] This is likely explained by the lower mucin content of Calu-3 mucus which falls below the overlap concentration of 2-4 mg/mL previously determined for mucins in a semi-dilute concentration regime.[28] At or above this overlap concentration, the spacing between neighboring mucin polymers is minimized to facilitate intermolecular (noncovalent) interactions to stabilize the mucus gel.[28] Based on measured mucin content (~1.5 mg/mL), Calu-3 mucus would be in a dilute concentration regime leading to reduced mucin-mucin interactions and greater mucus gel porosity. We also observed a tighter network structure in BCi mucus as compared to NHBE mucus. Based on the measured mucin and disulfide bond concentration (**Figure 1A, C**), we would have predicted a denser network to form in NHBE mucus in comparison to BCi mucus. However, this observation may be explained by differences in mucin glycosylation and/or mucin subtypes (e.g. MUC5B, MUC5AC) present in each gel type. For example, we have previously observed mucus gels composed of MUC5AC possess a smaller pore size in comparison to mucus gels composed of MUC5B.[29] Additional biochemical analyses will be needed in future work to explain these differences.

Our measurements of Udorn IAV diffusion in each mucus type revealed gels with smaller pores were more effective at virus trapping. This can be explained intuitively as mucus gels with narrower openings between mucin fibers can physically obstruct IAV diffusion. Based on the measured size range of Udorn IAV (**Fig. S1**), we estimate approximately 7%, 40%, and 24% of the measured pore sizes for Calu-3, BCi, and NHBE mucus, respectively, are small enough in size to sterically hinder diffusion and physically capture Udorn IAV within the mucus gel **(Figure 2C)**. This explains the observed differences in IAV diffusion in different mucus sources where BCi mucus, containing the largest fraction of virus-sized pores, posed the greatest hindrance to IAV mobility **(Figure 2D)**. While NHBE mucus possessed a far higher sialic acid content (**Figure 1B)**, NHBE mucus gels did not possess greater trapping capacity based on our measurements of IAV diffusion. Thus, our data suggests mucus network size has a significant impact on IAV mobility.

Consistent with prior reports,[10,30,31] we also found the enzymatic depletion of Sia alters mucus barrier function towards IAV **(Figure 3)**. Treatment with NA_{ex} depleted Sia in NHBE mucus by 8-fold without altering mucus network structure, as indicated by measured NP diffusion. Our results also indicated that removal of terminal Sia increased IAV mobility, compared to the untreated mucus **(Figure 3C)**. This is likely explained by a reduction in IAV-mucus binding due to the loss of Sia receptors that slow IAV diffusion. We also used a previously reported approach

to chemically remove Sia[11] from NHBE mucus that involves sodium periodate ($NaIO_4$) treatment to oxidize the bonds between adjacent hydroxyls of mucin-associated sugars. This resulted in a 2.3-fold decrease in Sia concentration **(Figure S2)**; however, both NP and Udorn diffused faster in $NaIO_4$-treated mucus compared to untreated mucus. The increased NP diffusion indicates increased pore size with $NaIO_4$ treatment which may also contribute to the observed increases in IAV diffusion.

To evaluate the importance of Sia binding preference, we utilized two Udorn mutants that preferentially bind either α2,3- or α2,6-Sia. Amongst the IAV with different Sia binding preferences, we observed a slower rate of diffusion for Ud23 IAV compared to Ud26 IAV, indicative of more trapping in NHBE mucus **(Figure 4B)**. This may be explained by a higher concentration of α2,3-Sia linkages in airway mucus as determined in previous work.[32–34] However, there were no significant differences in the estimated dissociation constants for the IAV in NHBE mucus **(Figure 4C)**. In addition, we predicted the highest total percentage of Udorn particles would cross the mucus barrier in the NHBE mucus **(Figure 4E-F, Supplemental Table 1)**. Interestingly, very similar fractions of Ud23 and Ud26 IAV particles are predicted to bypass the mucus barrier. These data suggest Sia preference has a relatively small impact on the protective functions of the mucus barrier against IAV. Udorn, Ud23, and Ud26 IAV diffusion was also evaluated in Calu-3 and BCi mucus where we observed increased diffusivity in Calu-3 compared to BCi mucus **(Figure S3)**. Interestingly, the dissociation constants for all IAV types in Calu-3 mucus were lower than in the BCi mucus, indicating greater association of the IAV to the mucus network with the largest pore size, as indicated by the muco-inert NP.

The findings of this study are in agreement with our previous work indicating that IAV mobility is dependent on the network size of the mucus, as opposed to IAV-mucus binding alone.[15] Overall, our data emphasizes the role of network size rather than glycan-specific interactions as responsible IAV movement. Sia present in the mucus gel was also found to enhance IAV trapping, but surprisingly, Sia binding preferences had less of a role in IAV-mucus interactions. The weak dependence of IAV on Sia preference could be attributed to the presence of primarily *O*-linked Sia in mucin, as opposed to primarily *N*-linked Sia on the surface of airway epithelial cells.[35] Direct profiling of HA binding to mucins and *O*-linked mucin glycan is likely needed to determine mucin-associated Sia preferences for IAV. We also note the glycan profile of the mucus barrier may be altered between individuals, as a function of age, and as a result of underlying lung disease.[36,37] Alterations to mucin glycans and their impacts on the mucus barrier towards IAV and other respiratory viruses should also be considered in future work. Overall, this work provides further insight into the functional role of mucus in IAV pathogenesis and zoonotic transmission.

LIMITATIONS OF THE STUDY

Our study had several limitations. The relative concentrations of α2,3- vs α2,6-Sia terminated mucin glycans were not quantitatively assessed in the mucus collected for these studies and this is likely to influence the results of our studies. The Udorn mutants used in this work possessed alterations in Sia preference for HA envelope proteins. Inclusion of a pseudo-typed IAV with matched NA and HA pairs with preference for α2,3- vs α2,6-linked Sia could give additional insights in future work. Further, inactivation of NA via mutation would allow for the analysis of the effect of HA activity on mobility independent of NA activity in future studies. We also

determined the fraction of Udorn, Ud23, Ud26 particles to cross the mucus barrier in Calu-3 and BCi mucus based on our machine learning based predictions **(Figure S4)**. However, in the Calu-3 mucus, a small number of particles are included in the machine learning-based trajectory analysis, n = 28 compared to n = 374 and n = 238 in BCi-NS1.1 and NHBE mucus, respectively **(Supplemental Table 1)**. In order to predict the diffusion mode of individual IAV, individual particles must be tracked for the entire duration of the experiment.[24] In conditions with fast-moving particles, many of the determined trajectories are shorter due to their rapid motion out of the focal plane and as a result, are not considered in our analysis. This unfortunately limits our ability to compare these predictions across mucus types.

ACKNOWLEDGEMENTS

This project was funded by the Burroughs Welcome Fund CASI (to G.A.D.), Cystic Fibrosis Foundation (BOBOLT23H0 to A.B.), the National Institutes of Health (R21 AI142050 to M.A.S. & G.A.D., R01 HL160540 to G.A.D., R01 HL151840 to M.A.S., T32 AI089621 to L.K., M.R., E.I.), and the National Science Foundation (CBET 2129624 to G.A.D & M.A.S.).

AUTHOR CONTRIBUTIONS

L.K. conceived, designed, and performed the research and led data analysis of virus movement and binding. E.M.E designed and performed experiments for removal of sialic acid. E.I. produced all viruses used for this study. A.B, M.A.I, and M.R. helped with experiments including human airway epithelial cell mucus collection. M.A.S. and G.A.D. conceived and designed experiments. L.K. and G.A.D. wrote the article. All authors reviewed and edited the article.

DECLARATION OF INTERESTS

The authors declare no competing interests.

EXPERIMENTAL PROCEDURES

Cell Culture

Human lung adenocarcinoma cells (Calu-3 cells) were purchased from ATCC (HTB-55). The immortalized HAE line BCi-NS1.1 was kindly provided by Matthew Walters and Ronald Crystal (Weill Cornell Medical College)[21]. Human airway tracheobronchial epithelial cells (NHBE) isolated from airway specimens from four donors without underlying lung disease were provided by Lonza, Inc.

BCi-NS1.1 and NHBE cells were first expanded on plastic in Pneumacult-Ex or Pneumacult-Ex Plus medium (no. 05008 or 05040, StemCell Technologies). Airway cells were then seeded (3.3 × 104 cells/well) on rat tail collagen type 1-coated permeable Transwell membrane supports (6.5 mm; no. 3470, Corning, Inc.) and differentiated in Pneumacult-ALI medium (no. 05001, StemCell Technologies) with provision of an air-liquid interface for approximately 6 weeks to form polarized cultures that resemble *in vivo* pseudostratified mucociliary epithelium.

Calu-3 cells were expanded and maintained in Eagle's Minimum Essential Medium (EMEM; ATCC) with 10% fetal bovine serum (FBS; Sigma-Aldrich) and 1% Penicillin-Streptomycin solution (Pen-Strep; Sigma-Aldrich). Cells were seeded on collagen-treated (Sigma Aldrich) PET 0.4 μm 24-well hanging inserts (EMD Millipore) for air-liquid interface (ALI) culturing. Cells were maintained in ALI for 25 days to allow for polarization and mucus production. All cell cultures were maintained at 37°C with 5% CO2.

Virus Strains

The reverse genetics system for influenza A virus A/Udorn/307/72 (Udorn), an H3N2 IAV that preferentially binds α2,6-Sia, was a gift from Robert Lamb. Infectious virus was rescued from cloned cDNAs in 293T and MDCK cells as previously described.[38]

Method Details

Influenza mutations and labeling

Two Udorn mutants were prepared according to previous works: Udorn with an HA mutation for preferential α2,3-Sia binding (Ud23), and Udorn with an HA mutation for preferential α2,6-Sia binding (Ud26)[20,39]. Ud23 has two mutations in the receptor binding domain, L226Q and S228G, while Ud26 has a single mutation in the receptor binding domain, E190D[20]. Udorn IAV was labeled with a lipophilic dye, 1,1′-dioctadecyl-3,3,3′,3′-tetramethylindocarbocyanine perchlorate (DiI; Invitrogen) while Ud23 and Ud26 IAV were labeled with a different lipophilic dye with a longer excitation and emission wavelength, 1,1′-dioctadecyl-3,3,3′,3′-tetramethylindodicarbocyanine 4-chlorobenzenesulfonate salt (DiD; Invitrogen). IAV sizes were determined **(Figure S4)** via dynamic light scattering (DLS) using the NanoBrook Omi (Brookhaven Instruments).

Nanoparticle preparation

As previously described, carboxylate modified fluorescent polystyrene nanoparticles (NP; Life Technologies) with a diameter of 100 nm were coated with 5 kDa methoxy polyethylene glycol (PEG)-amine (Creative PEGWorks) via a carboxyl-amine linkage to generate muco-inert nanoparticles.[40] NP sizes were determined **(Figure S4)** via DLS using the NanoBrook Omi (Brookhaven Instruments).

Airway epithelial cell mucus collection

Airway epithelial cell cultures were washed with phosphate buffered saline (PBS) to remove the accumulated mucus from the apical surface for collection. The collected mucus was filtered using Amicon ultra centrifugal filter units with a 100 kDa cutoff to remove excess PBS. The resulting mucus was stored at 4 °C until time of use. Mucus collected from NHBE cells was pooled for all experiments. The donor information for the NHBE cells is included in **Supplemental Table 2**.

Disulfide bond concentration assay

For mucus collected from Calu-3, BCi-NS1.1, and NHBE cells, the disulfide bond concentration was determined using a previously established protocol.[41] Briefly, samples were resuspended in 8 M Guanidine-HCl to bring the final volume to 500 μL before treatment with 10% (v/v) 500 mM iodoacetamide at room temperature for 1 hour. Samples were subsequently treated with 10% (v/v)

1 M DTT at 37 °C for 2 hours. Small molecules were removed by passing samples through 7 k MWCO Zebra desalting columns, which was also used to exchange the buffer for 50 mM Tris-HCl (pH 8.0). Equal volumes of sample and 2 mM monobromobimane were combined in a 96-well plate before incubation at room temperature for 15 minutes. The samples were read at 395 nm excitation and 490 nm emission and compared to a standard curve of L-cysteine to determine the disulfide bond concentration.

Mucin content assay

Using a previously established protocol,[42] mucus collected from Calu-3, BCi-NS1.1, and NHBE cells was analyzed to determine the relative mucin content. Briefly, 50 µL of samples were combined with 60 µL of alkaline CNA reagent, which was made by combining 200µL of 0.6 M 2-cyanoacetamide and 1 mL of 0.15 M NaOH. Samples were then incubated at 100 °C for 30 minutes. Subsequently, 0.5 mL of 0.6 M borate buffer, pH 8.0, was added to each sample. After samples cooled for 15 minutes at room temperature, the fluorescent intensity was measured at 336 nm excitation and 383 nm emission. Mucin from porcine gastric mucin was dissolved in mucin buffer and analyzed with this protocol to generate a standard curve. Mucin buffer was made by combining 0.01 M Na_2HPO_4 and 0.04% NaN_3 at pH 7.4.

Sialic acid concentration assay

Sialic acid (Sia) concentration was determined in mucus samples using a Sia assay kit (Sigma-Aldrich, MAK314) and following the manufacturer protocol. Briefly, samples were hydrolyzed to release bound Sia. These hydrolyzed samples were used to determine the total Sia concentration. Samples were then combined with thiobarbituric acid. Samples were oxidized, resulting in the oxidation of Sia into formylpyruvic acid, which reacts with thiobarbituric acid to form a pink product. The fluorescence of the product for each sample was measured at 555 nm excitation and 585 nm emission and compared to a standard curve of Sia to determine the Sia concentration in each sample.

Fluorescence imaging

To evaluate the movement of particles in HAE mucus, 1 µL of each type of particle was added to 20 µL of HAE mucus and placed on a slide in the middle of a vacuum grease-coated O-ring. Slides were equilibrated for 30 minutes at room temperature prior to fluorescence imaging with a Zeiss Confocal LSM 800 microscope equipped with a 63x water-immersion objective. Multiple 10-second videos were recorded at 33.3 frames per second for each sample.

Enzymatic alteration of mucus glycans

Collected NHBE mucus was incubated with 10 µL exogenous α2-3,6,8,9-Neuraminidase (NA_{ex}) from *Arthrobacter ureafaciens* (5 U/mL, Millipore Sigma) in 5 mL of reaction buffer (0.1 M sodium acetate, pH 5.5) for 2 hours at 37 °C. The treated samples were washed with PBS to remove NA_{ex} and biproducts before subsequent concentration via Amicon ultra centrifugal filter units with 100 kDa MW cutoff. Samples were then resuspended to original volume with PBS.

Chemical alteration of mucus glycans

Mucus collected from NHBE cells was incubated in 5 mL of reaction buffer (0.1 M sodium acetate, pH 5.5) with 2 mM ice-cold sodium periodate ($NaIO_4$) for 30 minutes at 4 °C while protected from

light. Unreacted sodium periodate was quenched with excess ethylene glycol. The treated samples were washed with PBS to remove reactant materials before subsequent concentration via Amicon ultra centrifugal filter units with 100 kDa MW cutoff. Concentrated samples were resuspended to original volume with PBS.

Quantification and Statistical Analysis

Multiple particle tracking analysis

Fluorescence microscopy video files were processed using a previously developed MATLAB code capable of tracking multiple particles and calculating the MSD. The MSD was calculated as $\langle \mathrm{MSD}(\tau) \rangle = \langle (x^2+y^2) \rangle$, for each particle.[43–45] The MSD values for NP were then used to calculate the microrheological properties using the generalized Stokes-Einstein relation,[46] as $G(s)=2k_BT/(\pi as\langle \Delta r^2(s) \rangle)$ gives the viscoelastic spectrum where k_BT is the thermal energy, a is the radius, and s is the complex Laplace frequency.[40] The complex modulus G^* was calculated as $G^*(\omega)=G'(\omega)+G''(i\omega)$ where $i\omega$ is used in place of s, i is a complex number, and ω is the frequency[18]. The pore size (ξ) can be estimated from the G' values as $\xi = (k_BT/G')^{1/3}$.[40]

Potential energy and dissociation analysis

Trajectories for individual IAV and NP were analyzed to determine the potential energy and dissociation constants using a previously described method.[15] Briefly, individual trajectories were recentered and the radial distance (r) from the center of the trajectory for each frame was calculated. The resulting r values were used to generate a histogram, which was normalized and the resulting counts in the histogram were used to calculate the potential energy using Equation 1,

$$\mathrm{U_{3D}/k_BT=-ln[n(r)/n_{max}]}, \quad (1)$$

where $n(r)$ is the number of counts in the normalized histogram for a given r value, and $n_{\max}$ is the largest count value.[47] The calculated potential energy profiles for IAV and NP were used to subtract the steric obstruction (U_s), accounted for in the NP, from the adhesive interactions of the IAV binding ($U_{B,IAV}$), to give the overall energy of confinement of IAV in a gel network ($U_{3D,IAV} = U_s + U_{B,IAV}$). From the $U_{B,IAV}$, the spring constant was calculated using Equation 2,

$$U_{B,IAV}/k_BT=0.5(k_s/k_BT)r^2, \quad (2)$$

where k_BT is thermal energy in pN•nm and k_s is in the units of pN/nm.[47] The resulting spring constant was subsequently used to calculate an effective dissociation constant using Equation 3,

$$\mathrm{K_{3D} = (2\pi k_BT/k_s)^{-3/2} \exp(-U_M/k_BT)}, \quad (3)$$

where U_M is the depth of energy well, which in this case was the measured $U_{B,IAV}$ (in pN•μm).[48] In addition to the potential energy, the recentered trajectories and their r values were used to calculate the measurement of confinement (σ) using Equation 4,

$$\sigma = \frac{2}{n}\sum_{i=1}^{n}|r_i|, \quad (4)$$

where r is the radial distance from the center of the trajectory and n is the number of frames.[15]

Machine learning based analysis for particle survival

Using the previously published machine learning-based analysis and the particle survival analysis,[24,25,27] the trajectory data for each viral strain and the muco-inert nanoparticles were analyzed to classify particle movement as fractional Brownian motion (FBM), Brownian motion. (BM), or continuous time random walk (CTRW). The resulting classified trajectories were used in the particle survival analysis to determine the percentage of particles that were predicted to cross the mucosal barrier. For each sample the median α and diffusivity values for particles exhibiting each type of motion were analyzed to determine the particle survival using the survival functions for diffusive and subdiffusive motion. The survival function for diffusive motion (S_D) is given in Equation 5,

$$S_D(t) = \frac{4}{\pi}\sum_{n=0}^{\infty}\left[exp\left(-\left(\frac{(2n+1)\pi}{2h}\right)^2 \mathcal{D}t^{\alpha}\right)\frac{(-1)^n}{2n+1}\right], \quad (5)$$

where $\mathcal{D}$ is the diffusion coefficient, α is the anomalous diffusion exponent, t is the time in seconds, and h is the distance to the absorbing boundary[25]. The survival function for sub-diffusive motion (S_{SD}) is given in Equation 6,

$$S_{SD}(t) = \frac{4}{\pi}\sum_{n=0}^{\infty}\left[E_{\alpha}\left(-\left(\frac{(2n+1)\pi}{2h}\right)^2 \mathcal{D}_{\alpha}t^{\alpha}\right)\frac{(-1)^n}{2n+1}\right], \quad (6)$$

where

$$E_{\alpha}(z) = \sum_{k=0}^{\infty}\frac{z^k}{\Gamma(1+\alpha k)} \quad (7)$$

is the Mittag-Leffler function.[25] For these calculations the mucus layer thickness was set to 10 μm and time in seconds was set to 2 h to determine the survival function within a physiologically relevant timeframe. The resulting survival function, $S(t)$, was then used to calculate the cumulative distribution function, (F), using Equation 8,

$$F(t) = 1 - S(t), \quad (8)$$

which determined the fraction of particles able to cross the absorbing boundary.[25] The percent of particles for each classification and the cumulative distribution function were used to calculate the percentage of particles capable of crossing the mucus barrier using Equation 9,[27]

$$\%\ particles\ across\ mucus\ barrier = F \times (\%\ particles). \quad (9)$$

REFERENCES

1. Linden, S.K., Sutton, P., Karlsson, N.G., Korolik, V., and McGuckin, M.A. (2008). Mucins in the mucosal barrier to infection. Mucosal Immunol *1*, 183–197. 10.1038/mi.2008.5.

2. Zanin, M., Baviskar, P., Webster, R., and Webby, R. (2016). The Interaction between Respiratory Pathogens and Mucus. Cell Host & Microbe *19*, 159–168. 10.1016/j.chom.2016.01.001.

3. Song, D., Cahn, D., and Duncan, G.A. (2020). Mucin Biopolymers and Their Barrier Function at Airway Surfaces. Langmuir. 10.1021/acs.langmuir.0c02410.

4. Werlang, C., Cárcarmo-Oyarce, G., and Ribbeck, K. (2019). Engineering mucus to study and influence the microbiome. Nature Reviews Materials, 1.

5. Thornton, D.J., Rousseau, K., and McGuckin, M.A. (2008). Structure and function of the polymeric mucins in airways mucus. Annu. Rev. Physiol. *70*, 459–486. 10.1146/annurev.physiol.70.113006.100702.

6. Lamblin, G., Degroote, S., Perini, J.M., Delmotte, P., Scharfman, A., Davril, M., Lo-Guidice, J.M., Houdret, N., Dumur, V., Klein, A., et al. (2001). Human airway mucin glycosylation: a combinatory of carbohydrate determinants which vary in cystic fibrosis. Glycoconj J *18*, 661–684. 10.1023/a:1020867221861.

7. Ehre, C., Worthington, E.N., Liesman, R.M., Grubb, B.R., Barbier, D., O'Neal, W.K., Sallenave, J.-M., Pickles, R.J., and Boucher, R.C. (2012). Overexpressing mouse model demonstrates the protective role of Muc5ac in the lungs. Proceedings of the National Academy of Sciences *109*, 16528–16533. 10.1073/pnas.1206552109.

8. Kudo, E., Song, E., Yockey, L.J., Rakib, T., Wong, P.W., Homer, R.J., and Iwasaki, A. (2019). Low ambient humidity impairs barrier function and innate resistance against influenza infection. Proc. Natl. Acad. Sci. U.S.A. *116*, 10905–10910. 10.1073/pnas.1902840116.

9. de Vries, E., Du, W., Guo, H., and de Haan, C.A.M. (2020). Influenza A Virus Hemagglutinin–Neuraminidase–Receptor Balance: Preserving Virus Motility. Trends in Microbiology *28*, 57–67. 10.1016/j.tim.2019.08.010.

10. Yang, X., Steukers, L., Forier, K., Xiong, R., Braeckmans, K., Reeth, K.V., and Nauwynck, H. (2014). A Beneficiary Role for Neuraminidase in Influenza Virus Penetration through the Respiratory Mucus. PLoS ONE *9*, e110026. 10.1371/journal.pone.0110026.

11. Cohen, M., Zhang, X.-Q., Senaati, H.P., Chen, H.-W., Varki, N.M., Schooley, R.T., and Gagneux, P. (2013). Influenza A penetrates host mucus by cleaving sialic acids with neuraminidase. Virol J *10*, 321. 10.1186/1743-422X-10-321.

12. Dadonaite, B., Vijayakrishnan, S., Fodor, E., Bhella, D., and Hutchinson, E.C. (2016). Filamentous influenza viruses. Journal of General Virology *97*, 1755–1764. 10.1099/jgv.0.000535.

13. Duncan, G.A., Jung, J., Hanes, J., and Suk, J.S. (2016). The Mucus Barrier to Inhaled Gene Therapy. Molecular Therapy *24*, 2043–2053. 10.1038/mt.2016.182.

14. Schuster, B.S., Suk, J.S., Woodworth, G.F., and Hanes, J. (2013). Nanoparticle diffusion in respiratory mucus from humans without lung disease. Biomaterials *34*, 3439–3446. 10.1016/j.biomaterials.2013.01.064.

15. Kaler, L., Iverson, E., Bader, S., Song, D., Scull, M.A., and Duncan, G.A. (2022). Influenza A virus diffusion through mucus gel networks. Commun Biol *5*, 249. 10.1038/s42003-022-03204-3.

16. Wang, Y.-Y., Harit, D., Subramani, D.B., Arora, H., Kumar, P.A., and Lai, S.K. (2017). Influenza-binding antibodies immobilise influenza viruses in fresh human airway mucus. European Respiratory Journal *49*, 1601709. 10.1183/13993003.01709-2016.

17. Lieleg, O., Lieleg, C., Bloom, J., Buck, C.B., and Ribbeck, K. (2012). Mucin Biopolymers As Broad-Spectrum Antiviral Agents. Biomacromolecules *13*, 1724–1732. 10.1021/bm3001292.

18. Wardzala, C.L., Wood, A.M., Belnap, D.M., and Kramer, J.R. (2022). Mucins Inhibit Coronavirus Infection in a Glycan-Dependent Manner. ACS Cent. Sci. *8*, 351–360. 10.1021/acscentsci.1c01369.

19. Matrosovich, M., Tuzikov, A., Bovin, N., Gambaryan, A., Klimov, A., Castrucci, M.R., Donatelli, I., and Kawaoka, Y. (2000). Early Alterations of the Receptor-Binding Properties of H1, H2, and H3 Avian Influenza Virus Hemagglutinins after Their Introduction into Mammals. J Virol *74*, 8502–8512. 10.1128/JVI.74.18.8502-8512.2000.

20. Pekosz, A., Newby, C., Bose, P.S., and Lutz, A. (2009). Sialic acid recognition is a key determinant of influenza A virus tropism in murine trachea epithelial cell cultures. Virology *386*, 61–67. 10.1016/j.virol.2009.01.005.

21. Walters, M.S., Gomi, K., Ashbridge, B., Moore, M.A.S., Arbelaez, V., Heldrich, J., Ding, B.-S., Rafii, S., Staudt, M.R., and Crystal, R.G. (2013). Generation of a human airway epithelium derived basal cell line with multipotent differentiation capacity. Respir Res *14*, 135. 10.1186/1465-9921-14-135.

22. Jiang, K., Yan, H., Rickert, C., Marczynski, M., Sixtensson, K., Vilaplana, F., Lieleg, O., and Crouzier, T. (2021). Modulating the Bioactivity of Mucin Hydrogels with Crosslinking Architecture. Adv. Funct. Mater. *31*, 2008428. 10.1002/adfm.202008428.

23. Kaler, L., Joyner, K., and Duncan, G.A. (2022). Machine learning-informed predictions of nanoparticle mobility and fate in the mucus barrier. APL Bioengineering *6*, 026103. 10.1063/5.0091025.

24. Jamali, V., Hargus, C., Ben-Moshe, A., Aghazadeh, A., Ha, H.D., Mandadapu, K.K., and Alivisatos, A.P. (2021). Anomalous nanoparticle surface diffusion in LCTEM is revealed by deep learning-assisted analysis. Proc. Natl. Acad. Sci. U.S.A. *118*, e2017616118. 10.1073/pnas.2017616118.

25. Erickson, A.M., Henry, B.I., Murray, J.M., Klasse, P.J., and Angstmann, C.N. (2015). Predicting First Traversal Times for Virions and Nanoparticles in Mucus with Slowed Diffusion. Biophysical Journal *109*, 164–172. 10.1016/j.bpj.2015.05.034.

26. Duncan, G.A., Jung, J., Joseph, A., Thaxton, A.L., West, N.E., Boyle, M.P., Hanes, J., and Suk, J.S. (2016). Microstructural alterations of sputum in cystic fibrosis lung disease. JCI Insight *1*. 10.1172/jci.insight.88198.

27. Kaler, L., Joyner, K., and Duncan, G.A. (2022). Machine learning-informed predictions of nanoparticle mobility and fate in the mucus barrier. APL Bioengineering *6*, 026103. 10.1063/5.0091025.

28. Bansil, R., Stanley, E., and Lamont, J.T. (1995). Mucin Biophysics. Annu. Rev. Physiol. *57*, 635–657.

29. Song, D., Iverson, E., Kaler, L., Boboltz, A., Scull, M.A., and Duncan, G.A. (2022). MUC5B mobilizes and MUC5AC spatially aligns mucociliary transport on human airway epithelium. Sci. Adv. *8*, eabq5049. 10.1126/sciadv.abq5049.

30. Cohen, M., Zhang, X.-Q., Senaati, H.P., Chen, H.-W., Varki, N.M., Schooley, R.T., and Gagneux, P. (2013). Influenza A penetrates host mucus by cleaving sialic acids with neuraminidase. Virology Journal *10*, 321. 10.1186/1743-422x-10-321.

31. Vries, E. de, Du, W., Guo, H., and Haan, C.A.M. de (2019). Influenza A Virus Hemagglutinin–Neuraminidase–Receptor Balance: Preserving Virus Motility. Trends in Microbiology *28*, 57–67. 10.1016/j.tim.2019.08.010.

32. Baos, S.C., Phillips, D.B., Wildling, L., McMaster, T.J., and Berry, M. (2012). Distribution of sialic acids on mucins and gels: a defense mechanism. Biophys J *102*, 176–184. 10.1016/j.bpj.2011.08.058.

33. Gagneux, P., Cheriyan, M., Hurtado-Ziola, N., Van Der Linden, E.C.M.B., Anderson, D., McClure, H., Varki, A., and Varki, N.M. (2003). Human-specific Regulation of α2–6-linked Sialic Acids. Journal of Biological Chemistry *278*, 48245–48250. 10.1074/jbc.M309813200.

34. Couceiro, J.N.S.S., Paulson, J.C., and Baum, L.G. (1993). Influenza virus strains selectively recognize sialyloligosaccharides on human respiratory epithelium; the role of the host cell in selection of hemagglutinin receptor specificity. Virus Research *29*, 155–165. 10.1016/0168-1702(93)90056-S.

35. Walther, T., Karamanska, R., Chan, R.W.Y., Chan, M.C.W., Jia, N., Air, G., Hopton, C., Wong, M.P., Dell, A., Malik Peiris, J.S., et al. (2013). Glycomic Analysis of Human Respiratory Tract Tissues and Correlation with Influenza Virus Infection. PLoS Pathog *9*, e1003223. 10.1371/journal.ppat.1003223.

36. Nicholls, J.M., Bourne, A.J., Chen, H., Guan, Y., and Peiris, J.M. (2007). Sialic acid receptor detection in the human respiratory tract: evidence for widespread distribution of potential

binding sites for human and avian influenza viruses. Respir Res *8*, 73. 10.1186/1465-9921-8-73.

37. Rose, M.C., and Voynow, J.A. (2006). Respiratory Tract Mucin Genes and Mucin Glycoproteins in Health and Disease. Physiological Reviews *86*, 245–278. 10.1152/physrev.00010.2005.

38. Fodor, E., Devenish, L., Engelhardt, O.G., Palese, P., Brownlee, G.G., and García-Sastre, A. (1999). Rescue of influenza A virus from recombinant DNA. Journal of virology *73*, 9679–9682.

39. Iverson, E., Griswold, K., Song, D., Gagliardi, T.B., Hamidzadeh, K., Kesimer, M., Sinha, S., Perry, M., Duncan, G.A., and Scull, M.A. (2022). Membrane-Tethered Mucin 1 Is Stimulated by Interferon and Virus Infection in Multiple Cell Types and Inhibits Influenza A Virus Infection in Human Airway Epithelium. mBio *13*, e01055-22. 10.1128/mbio.01055-22.

40. Duncan, G.A., Jung, J., Joseph, A., Thaxton, A.L., West, N.E., Boyle, M.P., Hanes, J., and Suk, J.S. (2016). Microstructural alterations of sputum in cystic fibrosis lung disease. JCI Insight *1*. 10.1172/jci.insight.88198.

41. Yuan, S., Hollinger, M., Lachowicz-Scroggins, M.E., Kerr, S.C., Dunican, E.M., Daniel, B.M., Ghosh, S., Erzurum, S.C., Willard, B., Hazen, S.L., et al. (2015). Oxidation increases mucin polymer cross-links to stiffen airway mucus gels. Sci. Transl. Med. *7*. 10.1126/scitranslmed.3010525.

42. Crowther, R.S., and Wetmore, R.F. (1987). Fluorometric assay of O-linked glycoproteins by reaction with 2-cyanoacetamide. Analytical Biochemistry *163*, 170–174. 10.1016/0003-2697(87)90108-4.

43. Crocker, J.C., and Grier, D.G. (1996). Methods of Digital Video Microscopy for Colloidal Studies. Journal of Colloid and Interface Science *179*, 298–310. 10.1006/jcis.1996.0217.

44. Schuster, B.S., Ensign, L.M., Allan, D.B., Suk, J.S., and Hanes, J. (2015). Particle tracking in drug and gene delivery research: State-of-the-art applications and methods. Advanced Drug Delivery Reviews *91*, 70–91. 10.1016/j.addr.2015.03.017.

45. Joyner, K., Yang, S., and Duncan, G.A. (2020). Microrheology for biomaterial design. APL Bioengineering *4*, 041508. 10.1063/5.0013707.

46. Mason, T.G., and Weitz, D.A. (1995). Optical Measurements of Frequency-Dependent Linear Viscoelastic Moduli of Complex Fluids. Phys. Rev. Lett. *74*, 1250–1253. 10.1103/PhysRevLett.74.1250.

47. Shabaniverki, S., and Juárez, J.J. (2017). Characterizing gelatin hydrogel viscoelasticity with diffusing colloidal probe microscopy. Journal of Colloid and Interface Science *497*, 73–82. 10.1016/j.jcis.2017.02.057.

48. Duncan, G.A., and Bevan, M.A. (2014). Colloidal potentials mediated by specific biomolecular interactions. Soft Matter *10*, 8524–8532. 10.1039/C4SM01300J.